

# Catalytic Cracking of *n*-Decane over NiO–MoO<sub>3</sub> Modified Pt/ZrO<sub>2</sub>–TiO<sub>2</sub>–Al<sub>2</sub>O<sub>3</sub> Catalyst with Different Al<sub>2</sub>O<sub>3</sub> Ratios<sup>1</sup>

Hua Zhang<sup>a</sup>, Xiongjian Li<sup>a</sup>, Yi Jiao<sup>d</sup>, Zhongzheng Wang<sup>c</sup>, Quan Zhu<sup>a,\*</sup>, Jianli Wang<sup>b</sup>, and Xiangyuan Li<sup>a</sup>

<sup>a</sup>College of Chemical Engineering, Sichuan University, Chengdu 610065, P. R. China

<sup>b</sup>College of Chemistry, Sichuan University, Chengdu 610064, Sichuan, P. R. China

<sup>c</sup>School of Aeronautics and Astronautics, Sichuan University, Chengdu 610065, P. R. China

<sup>d</sup>Xi'an Modern Chemistry Research Institute, Xi'an 710065, Shanxi, China

\*e-mail: qzhu@scu.edu.cn

Received May 28, 2016

**Abstract**—A series of ZrO<sub>2</sub>–TiO<sub>2</sub>–Al<sub>2</sub>O<sub>3</sub> composite oxides with different Al<sub>2</sub>O<sub>3</sub> ratios were prepared by coprecipitation method and used as the supports of Pt/NiO–MoO<sub>3</sub>/ZrO<sub>2</sub>–TiO<sub>2</sub>–Al<sub>2</sub>O<sub>3</sub> catalysts. Catalytic activities for *n*-decane cracking over these catalysts were evaluated under high temperature and high pressure conditions. Physicochemical characteristics of as-prepared catalysts were detected by using automatic adsorption instrument, X-ray diffractometer, temperature programmed reduction, and temperature programmed desorption techniques to characterize the catalysts and supports. The results indicated that the catalyst which contained 60 wt % Al<sub>2</sub>O<sub>3</sub> had the largest surface area and pore volume (152.7 m<sup>2</sup>/g and 0.39 mL/g, respectively), and also it possessed strongest medium and strong acidity as well as medium acidic density. Moreover, the catalyst with 60 wt % Al<sub>2</sub>O<sub>3</sub> exhibited better cracking performances compared with the others. The gas yields over Cat3 were 1.5 and 1.2 folds higher than that obtained from thermal cracking at 650 and 700°C, respectively. In addition, the heat sinks were improved 0.27 MJ/kg and 0.25 MJ/kg at 650 and 750°C, respectively.

**Keywords:** ZrO<sub>2</sub>–TiO<sub>2</sub>–Al<sub>2</sub>O<sub>3</sub> composite oxides, NiO–MoO<sub>3</sub> promoter, catalytic cracking, heat sink, coke, surface acidity

**DOI:** 10.1134/S0965544117080175

## INTRODUCTION

“Thermal barrier” is a major concern associated with hypersonic flight in recent years. Endothermic hydrocarbon fuel, which can not only act as an ideal coolant to reduce the heat load of the aircraft engine, but also can improve the propulsion efficiency, has drawn increasing attention [1, 2]. Over the past few decades, a number of researches have been conducted to obtain high chemical heat absorption, especially focusing on catalytic cracking [3].

The catalysts for cracking reaction mainly include noble metals, zeolites, and composite oxides. Among them, composite oxide catalysts which exhibit more desirable high-temperature stability, more satisfying surface acidity, and better textural properties, have been widely used in fuel cracking [4, 5]. The composite oxides of ZrO<sub>2</sub>–TiO<sub>2</sub> in general display higher surface area, better surface acidic properties, and stronger mechanical strength than pure ZrO<sub>2</sub> or TiO<sub>2</sub> [6]. However, the stability of ZrO<sub>2</sub>–TiO<sub>2</sub> as supports applied to kerosene cracking at higher temperature

(>750°C) should be further improved. In our previous studies, different content Al<sub>2</sub>O<sub>3</sub> with larger surface area and better thermal stability was introduced into ZrO<sub>2</sub>–TiO<sub>2</sub> composite oxides, and the ZrO<sub>2</sub>–TiO<sub>2</sub>–Al<sub>2</sub>O<sub>3</sub> composite oxides were used to the cracking of RP-3 jet fuel [7]. It was found that there is a close correlation between the cracking activity and their acidic properties. However, the details on acidity modulation are rarely reported, hence it is necessary to investigate the effect of acid density and acidity on cracking activity by means of additive adding.

It is reported that the selective catalytic reduction (SCR) activities of MoO<sub>3</sub>–CeO<sub>2</sub> catalysts can be enhanced by Brønsted acidities provided by amorphous MoO<sub>3</sub> structures, and further cobalt-molybdenum bimetallic catalysts were applied to Fischer-Tropsch synthesis, ammonia decomposition and hydrodesulfurization/hydrodenitrogenation (HDS/HDN) reactions [8]. Cooper et al. stated that the addition of Mo would enhance stronger acid sites as a consequence of the higher electron deficiency at the interface between the Co and Mo species [9]. Besides, nickel exhibits similar basic chemical proper-

<sup>1</sup> The article is published in the original.

ties and structure characteristics with Co element, and Ni-doped in HDS catalysts even achieved better performances than Co-doped catalysts [10]. Moreover, the surface acidity and reducibility can be modulated when the nickel collaborates with molybdenum to modify catalyst in Ref. [11], which is important for cracking reactions.

In order to give a deep insight into the relationship between the acidic property and catalytic activity, in this work, we investigated the influence of Ni–Mo promoted Pt/ZrO<sub>2</sub>–TiO<sub>2</sub>–Al<sub>2</sub>O<sub>3</sub> catalysts with varying Al<sub>2</sub>O<sub>3</sub> contents on the cracking of *n*-decane. The total and strong acid acidity of the catalysts were enhanced by the addition of molybdenum and nickel. The relationship between structure and catalytic activity was also investigated. This work provided some fundamental suggestions for the design of acid catalysts and promoter screening for the catalytic cracking of hydrocarbon under supercritical conditions.

## EXPERIMENTAL

### Composite Oxides and Catalysts Preparation

ZrO<sub>2</sub>–TiO<sub>2</sub>–Al<sub>2</sub>O<sub>3</sub> composite oxides (mass ratio of ZrO<sub>2</sub> : TiO<sub>2</sub> = 1 : 1) with different Al<sub>2</sub>O<sub>3</sub> mass ratios (0.0, 10.0, 60.0 wt %) were prepared by co-precipitation method. The precipitates were dried at 120°C and calcined at 600°C for 3 hours. Then the catalyst powders were prepared by sequential impregnation method. Firstly, the as-prepared supports were co-impregnated by a solution containing (NH<sub>4</sub>)<sub>6</sub>Mo<sub>7</sub>O<sub>24</sub> · 4H<sub>2</sub>O and Ni(NO<sub>3</sub>)<sub>2</sub> · 6H<sub>2</sub>O (MoO<sub>3</sub> content 10.0 wt % and NiO content 6.0 wt %), and then impregnated by chloroplatinic acid (Pt content 0.50 wt %). After each impregnation step, the samples were calcined for 2 hours at 500°C.

The powders were subsequently ball-milled with water to homogeneous slurry, and then coated on the inner walls of stainless-steel pipes using vacuum pump. The coated catalysts were dried overnight at 120°C, calcined at 500°C for 3 hours, labeled as Cat1, Cat2 and Cat3, with Al<sub>2</sub>O<sub>3</sub> mass ratio of 0, 0.1 and 0.6, respectively. The catalyst load of all catalysts is 0.2 ± 0.005 g/80 cm.

### Catalytic Activity Evaluation

The test apparatus used for cracking of *n*-decane under supercritical condition is shown in Fig. 1. It is composed of a fuel tank, tubular reactor, water condenser, gas-liquid separator, and an analysis system. The stainless-tubes (SS304 Φ3 × 0.5 mm, 800 mm length) coated with the as-prepared catalysts were used as reactors. The catalytic performance measurement was carried out from 600 to 750°C (fuel temperature at outlet), the pressure was kept at 2.5 MPa ( $P_c = 2.1$  MPa,  $T_c = 345^\circ\text{C}$  of *n*-decane), and the mass flow of *n*-decane was 1.0 g/s. The *n*-decane was pumped

into the electric heated reactor, and then the reacted fuel was cooled through the water condenser and separated by gas-liquid separator. In this process, the volume of gaseous product, the mass of liquid residues and the heat sinks were measured. Finally, the gaseous products were sampled and analyzed by on-line gas chromatography (GC, GC2000III, Shanghai Institute of Technology and Computing) equipped with TCD and FID detectors.

**Catalysts characterization.** N<sub>2</sub> adsorption/desorption analysis was conducted under -196°C using the Quadrasorb SI Automated Surface Area analyzer (Quantachrome Instruments, USA). The crystal structure of the samples were obtained by a power X-ray diffraction on a DX-2005 X-ray using Cu K<sub>α</sub> radiation ( $\lambda = 0.15406$  nm) and operating at 40 kV and 25 mV. The surface acidity of each catalyst was measured by NH<sub>3</sub> temperature programmed desorption (NH<sub>3</sub>-TPR) using a TP-5076 TPD instrument. The H<sub>2</sub> temperature programmed reduction (H<sub>2</sub>-TPR) of samples was performed on TP-5076 instrument equipped with a thermal conductivity detector (TCD).

## RESULTS AND DISCUSSION

### Catalytic Activity

**The distribution of gaseous product.** The main components in gaseous product are hydrogen, methane, ethane, ethylene, propane, propylene and C<sub>4</sub>, as shown in Table 1. As it can be seen, there are very small variations in components content along with the increase of Al<sub>2</sub>O<sub>3</sub> content in support. However, it is worth noting that the amount of low-carbon olefins (ethylene and propylene) and hydrogen over catalytic cracking is higher than thermal cracking. It is widely accepted that unsaturated hydrocarbons and hydrogen can provide more contribution to the heat absorption of fuels [12]. Thus, this may be one of the reasons that why catalytic cracking presented excellent heat sink which will be discussed later. Besides, the formation of a large number of small molecule hydrocarbons slows down ignition delay [13].

The gas yield and heat sink of the experimental system are expressed as follows:

$$x = \frac{m_1}{m_1 + m_2} \times 100\%, \quad (1)$$

$$P_{\text{in}} = q_m \Delta h + P_{\text{loss}}, \quad (2)$$

where  $x$  is gas yield of *n*-decane,  $m_1$  and  $m_2$  represent the mass of the gas and liquid residues, respectively.  $P_{\text{in}}$  is the input power of the electrical heater,  $q_m$  the mass flow rate of *n*-decane,  $\Delta h$  the heat sink of unit fuel of mass, and  $P_{\text{loss}}$  the heat loss that can be minimized through insulation measures.

The gas yields and heat sinks of thermal cracking and catalytic cracking at different temperatures are

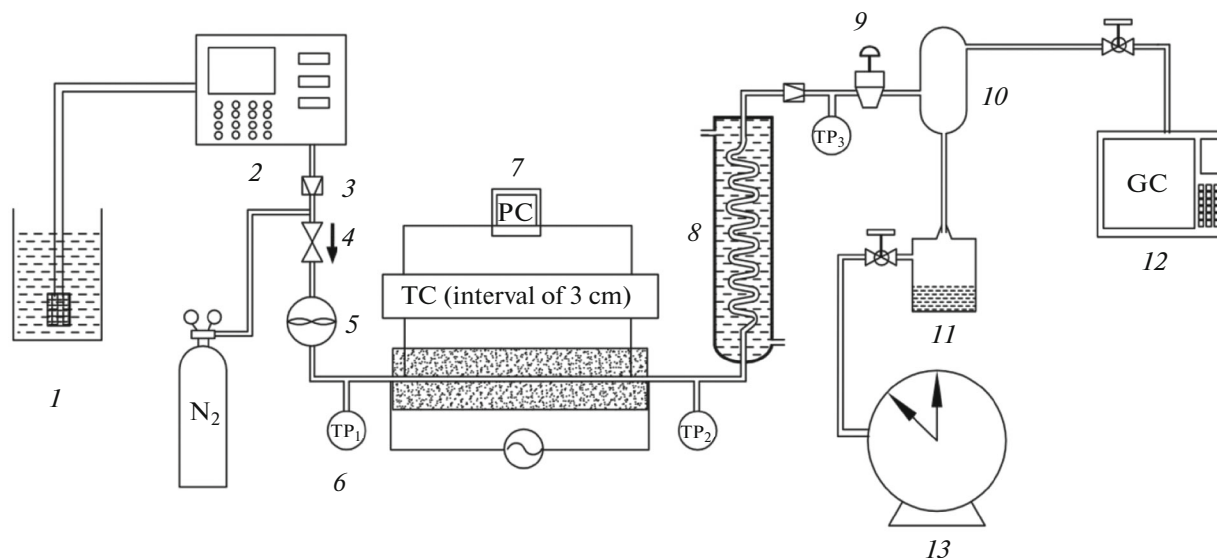


**Fig. 1.** The schematic diagram of apparatus: 1, fuel tank; 2, high pressure metering pump; 3, check valve; 4, three-way valve; 5, mass flow meter; 6, pressure and temperature control system; 7, thermocouple; 8, water condenser; 9, back pressure valve; 10, gas-liquid separator; 11, liquid receiver; 12, gas chromatograph; 13, wet gas flow meter.

shown in Fig. 2a,b, respectively. It is obviously that the gas yields and heat sinks over catalysts are higher than that produced from thermal cracking at the same experimental condition. Among the catalysts, Cat3 shows stable and preferable catalytic activity in the whole experimental temperature range. The gas products produced over Cat3 are 1.5 and 1.3 folds higher than thermal cracking at 650 and 700°C, respectively. And the heat sinks increase by 0.27 MJ/kg and 0.25 MJ/kg correspondingly. At lower temperature (<650°C), the catalytic activity over Cat2 is the highest from the point of gas yield and heat sink. However, the experiment by Cat2 was forced to stop above 650°C because of the serious coke blocking, which might be due to the too strong acidic sites of the catalyst. Also, Cat1 cannot be used at high temperature and the reason is possibly the same [5]. Above all, it is indicated that the catalyst with 60 wt % Al<sub>2</sub>O<sub>3</sub> has not only excellent thermal stability but also more positive inhibiting ability of coking formation.

**Coking inhibition.** To investigate the coking growth on the monolithic catalysts, the flow resistance was

monitored through the differential pressure between the inlet and outlet of the tubular reactor [14]. As shown in Fig. 3, the differential pressure of the thermal cracking is generally lower than those over the catalysts during the whole experimental run. It is well known that the number of acid sites and the distribution of them are important factors for cracking activity also for catalyst coking deactivation. High acid site density and strong acid sites may result in long carbenium ion residence time on the surface, and then the carbenium ions would undergo bimolecular reactions more readily, leading to serious carbon deposition. Therefore, with the introduction of catalysts, the amount of carbon increased in different degree [18]. Especially Cat2 exhibit highest coke formation among all experiments, it soared to 0.6 MPa even around 675°C, which is the reason why the experiment over Cat2 was forced to stop and confirmed by catalytic activity. Besides, among all the catalysts, Cat3 performs the perfect anti-coking capacity.

**Textural properties of catalysts.** Table 2 summarizes the specific surface area, pore volume, and average

**Table 1.** The distribution of gas product from thermal and catalytic cracking of *n*-decane at 700°C

<i>T</i> , °C	Samples	Mol fraction, %						
		H <sub>2</sub>	CH <sub>4</sub>	C <sub>2</sub> H <sub>6</sub>	C <sub>2</sub> H <sub>4</sub>	C <sub>3</sub> H <sub>8</sub>	C <sub>3</sub> H <sub>6</sub>	C <sub>4</sub>
700	Thermal	4.2	18.2	16.9	34.6	4.4	16.1	4.9
	Cat1	5.7	20.2	15.9	35.6	3.2	16.6	3.9
	Cat2	5.2	19.3	15.5	35.3	3.2	16.3	5.2
	Cat3	5.4	18.5	14.8	35.2	3.1	16.5	8.4

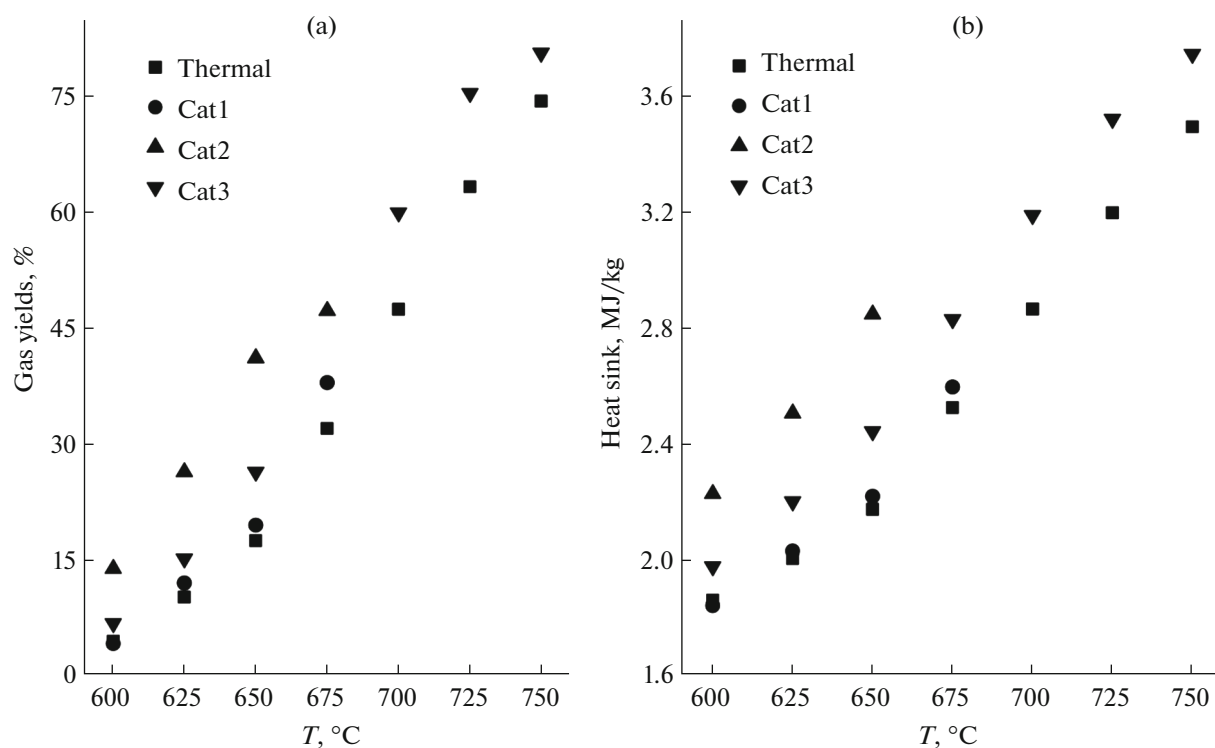


Fig. 2. The catalytic activity of thermal cracking and catalytic cracking: (a) gas yield (b) heat sink.

pore diameter of the as-prepared catalysts. As can be observed, the specific surface areas and pore volumes increase obviously with the increasing of Al<sub>2</sub>O<sub>3</sub> content, with maximized surface area Al<sub>2</sub>O<sub>3</sub> content of 60 wt % (152.7 m<sup>2</sup>/g and 0.39 mL/g). A large surface area is beneficial to the catalytic activity due to the uniform disperse of active sites, small size of active

centers, and reduction of aggregation of active sites. N<sub>2</sub> adsorption data show that the ZrO<sub>2</sub>–TiO<sub>2</sub>–Al<sub>2</sub>O<sub>3</sub> samples present typical type IV adsorption isotherms in conjunction with a H2-shaped hysteresis loop (as per the IUPAC classification), indicating that there are both slit and bottle-type pore shapes. Besides, the pore sizes of samples calculated by BJH method are less than 7.5 nm, and both slit or bottle-type pore shapes and mesoporous pore size distribution are beneficial to high space velocity reactions [15].

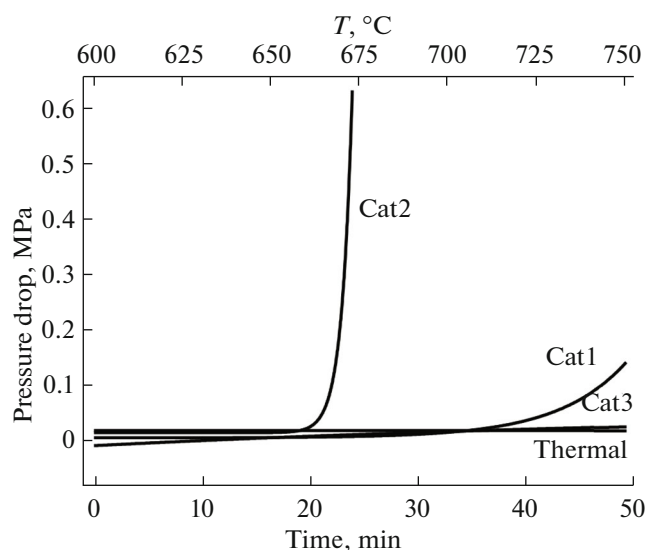


Fig. 3. The pressure drop of thermal and catalytic cracking.

**XRD results.** The XRD patterns are presented in Fig. 4. The complete ZrTiO<sub>4</sub> and anatase TiO<sub>2</sub> crystal phase are formed in Cat1 (ZrO<sub>2</sub>–TiO<sub>2</sub>), while Cat2 and Cat3 exist as basic amorphous structures. No crystal phases were observed after the addition of Al<sub>2</sub>O<sub>3</sub>, and the possible explanation is that Al<sup>3+</sup> prevents the agglomeration of Zr<sup>4+</sup> and Ti<sup>4+</sup> during the co-precipitation process. It is worth noting that the crystallization of supports will seriously affect the surface area and acidity, which is consistent with the results of BET and NH<sub>3</sub>-TPD test. Besides, no diffraction peaks of PtO, NiO, and MoO<sub>3</sub> are observed in Cat2 and Cat3, which might due to the low loading of Pt and high disperse of oxides on the surface of the catalysts [16]. The high degree of disperse could promote the catalytic activity, which agrees well with the experimental results. XRD results show that the addition of Al<sub>2</sub>O<sub>3</sub> could effectively shift the crystallization temperature of ZrO<sub>2</sub> and ZrTiO<sub>4</sub> crystal phases, which reduces the

**Table 2.** The textural performance of catalysts

Samples	Surface are, m <sup>2</sup> /g	Pore volume, mL/g	Average pore diameter, nm
Cat1	83.5	0.29	7.1
Cat2	135.2	0.34	5.7
Cat3	152.7	0.39	4.5

**Table 3.** Acidic sites concentration (mmol/g) of the prepared catalysts

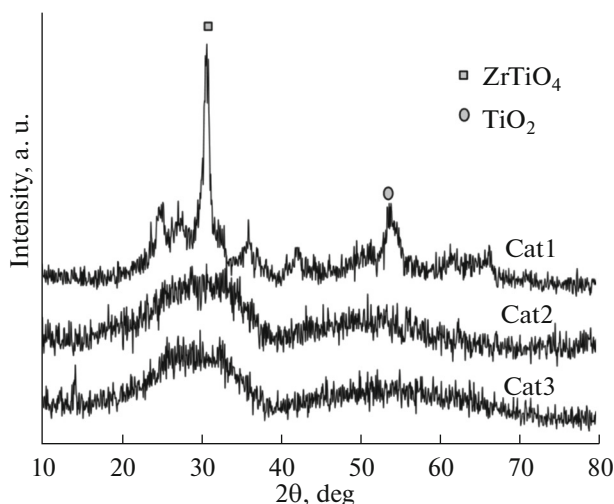
Catalysts	Weak acid sites	Medium acid sites	Strong acid sites	Total acid sites
Cat1	0.295	0.161	0.376	0.832
Cat2	0.667	0.120	0.329	1.016
Cat3	0.790	0.173	0.431	1.394

degradation of surface area and acidity and thus improves the catalytic activity.

**NH<sub>3</sub>-TPD results.** The NH<sub>3</sub>-TPD plots obtained from different samples are presented in Fig. 5. Absorbed NH<sub>3</sub> continuously stripped from the surfaces of catalysts, indicating that the distribution of the surface acidic sites is homogeneous and continuous, and there are many types of surface acidity. All the patterns show the weak acid desorption peak (100–350°C) and medium acid desorption peak (350–500°C) as well as strong acid desorption peak (500–800°C) [17]. Tables 3 and 4 present the acidic distributions and density of these catalysts, respectively. It is reported that the catalytic cracking of hydrocarbon is likely to proceed via classical carbenium ions formed on acid sites of the catalysts [3]. When the fraction of C–C bond tends to proceed at strongly acid sites, the hydrogen transfer reaction competing with C–C bond rupture can carry out at different acid centers (weak, medium and strong acid). What is more, the hydrogen transfer reaction is one of the important reactions of carbon deposition. Besides, report [18] stated that high acid site density and strength may result in long carbenium ion residence time on the surface, then the carbenium ions will undergo bimolecular reactions more readily, and hence leads to serious carbon deposition. Thus, numerous strong acid sites is beneficial to cracking of hydrocarbon, but high density of strong acid centers would lead to rapid coking. One can readily see that such opposite effect results in the supposition that coke formation and cracking activity reach an optimum combination at some intermediate density and amount of strong acid sites. As can be seen from Table 3, the total amount of acid sites increases obviously with the increased level of Al<sub>2</sub>O<sub>3</sub>, in which Cat3 has the largest acidic amount (1.394 mmol/g), which is favorable to cracking. Table 3 gives densities of different acid centers in each catalyst. Here we can see that Cat1 has the largest concentration of total and strong acid sites, 9.96 μmol/m<sup>2</sup> and 4.5 μmol/m<sup>2</sup> respectively. This might be the reason why Cat1 goes

through rapid coking. In contrast, Cat3 possesses moderate total and strong acid sites densities. Table 4 summarizes the percentages of various acid sites account for total acidic amount, and we see that the acidic property of Cat3 is in the middle zone among all the catalysts. In conclusion, the desirable amount and concentration of strong acid centers of Cat3 result in its better catalytic performances.

**H<sub>2</sub>-TPR results.** Figure 6 gives out the H<sub>2</sub>-TPR plots of prepared catalysts. The results reveal that there are several oxide species in the catalysts, and the support composition has a significant impact on the formation of them. Among all the plots, there is a broad and weak peak at low temperature (~242°C), which can be attributed to the reduction of free NiO and Pt on the catalytic surface [15]. In relative high temperature region (>400°C), a large reduction peak is observed around 610°C with regard to Cat1, indicating the existence of MoO<sub>3</sub> and superficial NiMoO<sub>4</sub> species [19]. For Cat2 and Cat3, there are two obvious

**Fig. 4.** XRD profiles of different catalysts.

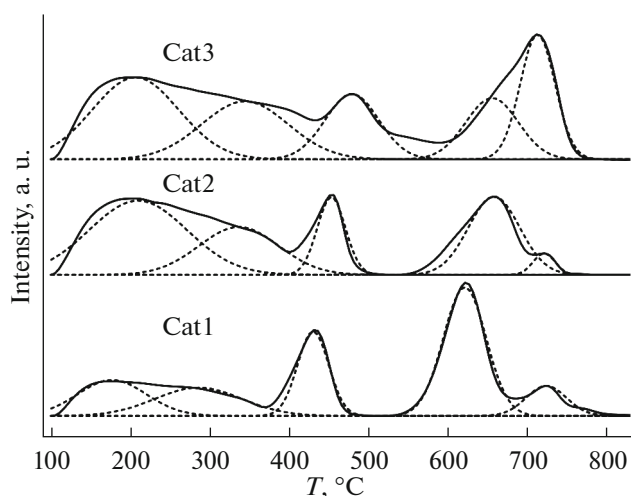


Fig. 5. NH<sub>3</sub>-TPD patterns for different catalysts.

reduction peaks at the range of 400–850°C. The peak centered at 515°C belongs to superficial NiMoO<sub>4</sub> species and MoO<sub>3</sub> mentioned in Cat1. The other around 750°C is caused by Al<sub>2</sub>(MoO<sub>4</sub>)<sub>3</sub> species and NiAl<sub>2</sub>O<sub>4</sub> spinel or NiAl<sub>2</sub>O<sub>4</sub>-like aluminate species [10]. The slight distinction among each catalyst in this region may be caused by two possible reasons. One is related to the formation of new species. When Al<sub>2</sub>O<sub>3</sub> was doped into ZrO<sub>2</sub>–TiO<sub>2</sub> support, it can interact with MoO<sub>3</sub> and NiO then resulted in the formation of Mo–O–Al bond and NiAl<sub>2</sub>O<sub>4</sub> spinel as well as NiAl<sub>2</sub>O<sub>4</sub>-like species. These species are more difficult to be reduced than NiMoO<sub>4</sub> species, thus the high temperature peak splitting into two obvious peaks [20]. Another reason is the amount of new species derived from the interaction between Al<sub>2</sub>O<sub>3</sub> and MoO<sub>3</sub>/NiO. With the increases of Al<sub>2</sub>O<sub>3</sub> content, more NiAl<sub>2</sub>O<sub>4</sub> or NiAl<sub>2</sub>O<sub>4</sub>-like species will be formed, and the reducibility of NiAl<sub>2</sub>O<sub>4</sub> spinel is better than that MoAl<sub>2</sub>O<sub>4</sub> species. Therefore, the reduction peak area of Cat3 around 750°C is larger than Cat2, and the maximum temperature moved to 736°C. Above all, the H<sub>2</sub>-TPR results illustrate that the addition of Al<sub>2</sub>O<sub>3</sub> reduces the synergy between Mo and Ni, and improves the reduction performance of catalyst [21], eventually enhances the reducibility of the catalysts. Moreover, the diminished

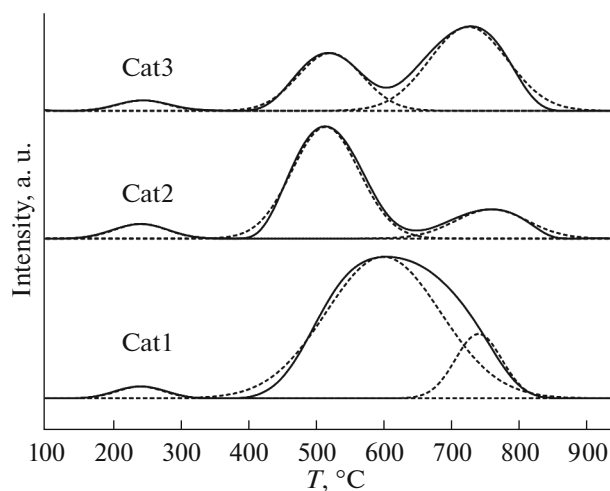


Fig. 6. The H<sub>2</sub>-TPR profiles of as-prepared catalysts.

interaction between Mo and Ni may result in less NiMoO<sub>4</sub> species, in other words, the excess strong acid sites will decrease, which is unanimous with the results of NH<sub>3</sub>-TPD.

## CONCLUSIONS

In conclusion, in NiO–MoO<sub>3</sub> modified catalysts, different content of Al<sub>2</sub>O<sub>3</sub> brings about the formation of different species on the surface of catalysts, and the surface acid sites are tuned for this reason. The Cat3 has the highest surface area (152.7 m<sup>2</sup>/g), pore volume (0.39 mL/g), and moderate concentration of strong acid (0.431 mmol/g, account for 31% of the total). All these factors facilitate the catalytic cracking reactions, and hence lead to a higher gas yield and heat sink. Therefore, surface loading with Cat3 is a potential catalyst pattern in active cooling of hypersonic flights.

## ACKNOWLEDGMENTS

The research was supported by the National Natural Science Foundation of China (91441132) and the Program for New Century Excellent Talents in University of Ministry of Education of China (NCET-13-0398).

Table 4. Acidic sites density (μmol/m<sup>2</sup>) of the prepared catalysts

Catalysts	Weak acid sites	Medium acid sites	Strong acid sites	Total acid sites
Cat1	3.53	1.93	4.5	9.96
Cat2	4.93	0.89	1.69	7.51
Cat3	5.17	1.13	2.82	9.13

## REFERENCES

1. I. W. Kay, W. T. Peschke, and R. N. Guile, *J. Propul. Power* **8**, 507 (1992).
2. F. Zhong, X. Fan, G. Yu, J. Li, and C. J. Sung, *J. Thermophys. Heat Transfer* **25**, 450 (2011).
3. T. Edwards, *Combust. Sci. Technol.* **178**, 307 (2006).
4. D. Mao and G. Lu, *J. Solid State Chem.* **180**, 484 (2007).
5. Y. Jiao, L. X. Qin, J. Wang, J. L. Wang, Q. Zhu, Y. Q. Chen, and X. Y. Li, *Acta Phys. Chim. Sin.* **27**, 2255 (2013).
6. B. Reddy and A. Khan, *Cat. Rev. Sci. Eng.* **47**, 257 (2005).
7. Y. Jiao, A. Liu, C. Li, J. Wang, Q. Zhu, X. Li, and Y. Chen, *Anal. Appl. Pyrolysis* **111**, 100 (2015).
8. Y. Z. Xiang and X. N. Li, *Chin. J. Chem. Eng.* **13**, 696 (2005).
9. C. G. Cooper, T. H. Nguyen, Y. J. Lee, K. M. Hardiman, T. Safinski, F. P. Lucien, and A. A. Adesina, *Catal. Today* **131**, 255 (2008).
10. T. Borowiecki and A. Golebiowski, *Catal. Lett.* **25**, 309 (1994).
11. W. Cheng, Y. M. Li, R. J. Wang, and J. Y. Zhang, *Chem. Ind. Eng.* **15**, 30 (1998).
12. H. Zhang, Z. Z. Wang, S. S. Li, Y. Jiao, J. L. Wang, Q. Zhu, and X. Y. Li, *Appl. Therm. Eng.* **111**, 811 (2007).
13. T. Edwards, *J. Propul. Power* **19**, 1089 (2003).
14. X. J. Li, H. Zhang, B. Liu, Q. Zhu, J. L. Wang, and X. Y. Li, *Appl. Therm. Eng.* **102**, 1238 (2016).
15. Y. Wang, H. Xu, H. Shang, M. Gong, and Y. Chen, *J. Energ. Chem.* **23**, 461 (2014).
16. M. Laniecki, M. Malecka-Grycz, and F. Domka, *Appl. Catal. A: Gen* **196**, 293 (2000).
17. Y. Jiao, J. Wang, Q. Zhu, X. Li, and Y. Chen, *Chin. J. Catal.* **35**, 175 (2014).
18. K. A. Cumming and B. W. Wojciechowski, *Catal. Rev.* **38**, 101 (2006).
19. G. Munuera, A. R. Gonzalez-Elipe, and J. P. Espings, *Surf. Sci.* **211**, 1113 (1989).
20. B. Chen, J. L. Falconer, K. M. Bailey, and B. Sen, *Appl. Catal.* **66**, 283 (1990).
21. A. A. Andreev, V. J. Kafedjiysky, and R. M. Edreva-Kardjieva, *Appl. Catal., A* **179**, 223 (1999).